Nonlinear Dyn (2017) 87:1617–1627
DOI 10.1007/s11071-016-3137-y

ORIGINAL PAPER

Nonlinear dynamics of an SMA-pendulum system

Dimitri D. A. Costa · Marcelo A. Savi

Received: 12 April 2016 / Accepted: 7 October 2016 / Published online: 15 October 2016

Abstract Pendulum is a simple system that is usually related to great discoveries in science and technology. Nonlinear dynamics of pendulum systems is related to a variety of responses being the objective of studies of oscillations, bifurcations and chaos. Smart material nonlinear effects are employed in several applications due to their adaptive behavior presenting great advantages in control strategies. This work deals with the dynamics of an SMA-pendulum system that consists of a pendulum coupled with shape memory alloy springs. A numerical investigation is carried out exploiting the temperature-dependent behavior of the SMA. Complex responses are presented and the possibility of thermal control of the system is investigated.

Keywords Nonlinear dynamics · Chaos · Shape memory alloys · Pendulum · Control

1 Introduction

Pendulum systems are extensively analyzed due to a variety of reasons, being a source of motivation for several discoveries in nonlinear dynamics and other fields of engineering [1,2]. DE PAULA et al. [3] discussed some aspects of pendulum dynamics, presenting an experimental-numerical investigation of a typical mechanical apparatus. Results show several complex responses that include bifurcations, chaos and transient chaos. Nonlinear control of these systems are investigated in several references, and it should be highlighted the use of either fuzzy logic or chaos control approaches [4–6]. Pendulum-like systems are also employed to model biological systems as in SUZUKI et al. [7] that describes the control of an ankle, model motor systems as treated in [8] and cranes according to the work of Ju et al. [9].

Smart materials represent a class of advanced materials with remarkable properties conferred by the coupling between different physical fields. Usually, they are employed for control purposes due to their adaptive capacity. Shape memory alloys (SMAs) belong to this class, presenting interesting properties for applied dynamics [10]. In this regard, applications in vibration control [11], origami structures [12], robotics [13] and energy harvesting [14] are possible being associated with a great variety of fields. The unique behavior of SMAs is due to the thermoelastic martensitic transformations that imply some of their traditional effects as pseudoelasticity and shape memory effect. The first one is identified as a complete strain recovery of the material with a hysteretic behavior in a loading-unloading cycle. On the other hand, shape memory effect is the ability to completely recover an amount of residual strain after a proper thermomechanical loading process. These characteristics can be used in bio-

D. D. A. Costa · M. A. Savi (✉)
Center for Nonlinear Mechanics/COPPE, Department of Mechanical Engineering, Universidade Federal do Rio de Janeiro, P.O. Box 68.503, Rio de Janeiro, RJ 21.941.972, Brazil
e-mail: savi@mecanica.ufrj.br

engineering, robotics, aerospace engineering, shape and vibration control, among others [12–17]. Synergistic use of smart materials has been increasing by exploring the proper characteristics of each material involved. SMA-piezoelectric systems are good examples for enhance energy harvesting capacity combining different characteristics of smart materials [14,18,19].

This work deals with the nonlinear dynamics of an SMA-pendulum system composed of a nonlinear pendulum coupled with SMA springs. This system has adaptive behavior, presenting a temperature-dependent response. Dynamical investigation is carried out pointing to some advantages of the use of SMA elements as well as some possible control applications.

2 SMA-pendulum system

Consider a pendulum system that consists of a disk with diameter D with a lumped mass m. The excitation of the pendulum is provided by a DC motor, with an arm of length b, connected to a string-spring system. The idea is to use a non-slipping string that is coiled on the pendulum through a disk of diameter d, being connected to SMA springs. A magnetic device provides dissipation to the system. The system is similar to the one discussed by DE PAULA et al. [3] that established a comparison between theory and experiment, with very good results. Here, the system is modified throughout the use of SMA springs for the excitation mechanism (Fig. 1).

By considering that ϕ is the angle of the pendulum, and assuming that dissipation is a combination of linear viscous and dry friction, respectively, represented by coefficients ϑ and μ, the equation of motion is given by

$$\phi'' = -\frac{\vartheta}{I\omega_0}\phi' - \frac{\mu}{mgD}\text{sign}\left(\phi'\right) - \frac{\sin\left(\phi\right)}{2} + \frac{d}{2mgD}\left(F_m - s_m\right) \tag{1}$$

where I is the angular inertia of the pendulum, g is the acceleration of gravity, and ω_0 is a reference frequency defined as follows,

$$\omega_0 = \sqrt{\frac{mgd}{I}} \tag{2}$$

Time derivative $()'$ is related to dimensionless time defined by $t^* = t\omega_0$. Moreover, s_m is the force of the anchored spring and F_m is the excitation force of the motor-string-spring system.

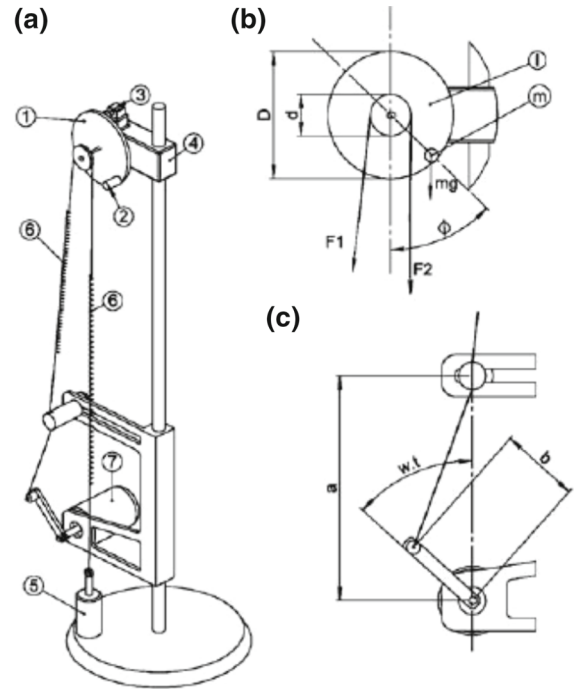

Fig. 1 Nonlinear pendulum: **a** physical model (*1*) metallic disk; (*2*) lumped mass; (*3*) magnetic damping device; (*4*) rotary motion sensor; (*5*) anchor; (*6*) SMA spring; (*7*) electric motor. **b** Parameters and forces on the metallic disk. **c** Parameters for driving device [3]

The geometric displacement due to the motor movement is given by:

$$y = \sqrt{\left(a^2 + b^2 - 2ab\cos\left(\frac{\omega t^*}{\omega_0} + \theta\right)\right)} - (a - b) - \frac{d\phi}{2} \tag{3}$$

where a is the distance between the center of the disk and the center of the rotor, θ is the initial phase of the motor, ω is the excitation frequency and b is the motor arm length.

Different models can be employed to describe the thermomechanical behavior of SMAs [20–22], and specifically for springs [20,23]. Polynomial model is the simplest alternative that capture the general thermomechanical behavior of SMAs, being interesting to be employed for the qualitative description of dynamical systems. This model adopts a stress–strain ($\sigma - \varepsilon$) relation as follows,

$$\sigma = a_m^* (T - T_M)\,\varepsilon - b_m^* \varepsilon^3 + \frac{b_m^* 2}{a_m^* (T_A - T_M)}\varepsilon^5 \quad (4)$$

where a_m^* and b_m^* are material parameters, T_M is the temperature below which only martensitic phase is stable, T_A is the temperature above which only austenitic phase is stable (at stress-free scenario), T is the temperature.

The definition of the polynomial constitutive equation is based on stabilities of the SMA phases. Basically, this choice is based on the existence of three macroscopic phases: austenite (A) and two variants of martensite (tension, M+, and compression, M−). In this regard, SMA has two stable phases for low temperature, below T_M, representing two martensitic variants; three stable phases for intermediate temperature ($T_M < T < T_A$), representing two martensitic variants and austenite; and just one stable phase for high temperature (above T_A) representing austenite. Hence, polynomial model is defined considering a free energy that is represented by a sixth order polynomial as a function of strain and temperature. Figure 2 presents free energy curves together with stress–strain curves for three different representative temperatures. Note that phase transformations are associated with the variations of these curves, which allows a qualitative description of SMA response. The simplicity of this model comes from the fact that no other extra internal variables are employed to describe phase transformations.

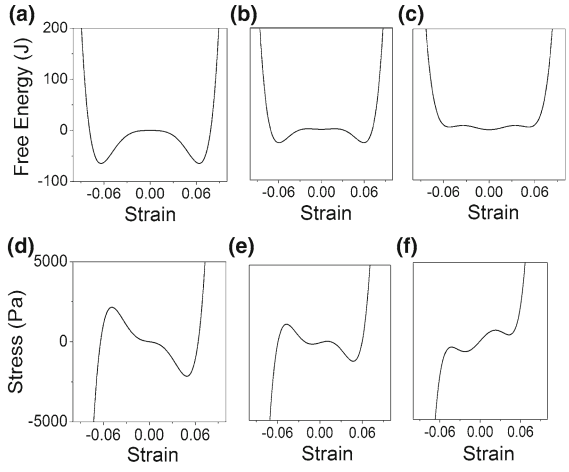

Fig. 2 SMA polynomial constitutive model: free energy potential (*upper panel*) and stress–strain curves (*lower panel*). **a**, **d** $T < T_M$; **b**, **e** $T_M < T <$; **c**, **f** $T > T_A$

The description of the spring behavior is done assuming that phase transformation is homogeneous for the spring cross-section. Based on that, it is possible to write a force-displacement equation that is formally similar to the stress–strain expression [20]. Hence, the terms related to the equations of motion, Eq. (1), can be written as follows,

$$F_m = a_m (T - T_M)\, y - b_m y^3 + \frac{b_m^2}{a_m (T_A - T_M)} y^5 \quad (5)$$

$$s_m = a_m (T - T_M)\frac{\phi d}{2} - b_m \left(\frac{\phi d}{2}\right)^3 + \frac{b_m^2}{a_m (T_A - T_M)}\left(\frac{\phi d}{2}\right)^5 \quad (6)$$

Numerical simulations are performed to investigate the nonlinear dynamics of the SMA-pendulum system. Fourth-order Runge–Kutta method is employed and Lyapunov exponents are calculated using the algorithm proposed by WOLF et al. [24]. Parameters employed for simulations follows the experimental results presented in reference [3]: $m = 1.47\,\text{kg}$, $D = 9.5\,\text{cm}$, $d = 4.8\,\text{cm}$, $b = 6\,\text{cm}$, $a = 16\,\text{cm}$, $\mu = 1.27210^{-4}\,\text{Nm}$, $\vartheta = 2.368\,\frac{\text{kgm}^2}{\text{s}}$, $g = 9.81\,\text{m/s}^2$. SMA parameters are adjusted with experimental data: $T_A = 289.35\,\text{K}$, $T_M = 282.45\,\text{K}$, $a_m = 0.4375\,\text{N/mK}$ and $b_m = 150\,\text{Pa/m}$.

The next sections present numerical simulations considering three parts. Initially, free vibration is analyzed, exploring the structure of equilibrium points. Afterward, forced vibration is treated showing complex responses as chaos and transient chaos. Finally, temperature variations are employed for control purposes.

3 Free vibration

Initially, the structure of equilibrium points is analyzed, giving special attention to its temperature-dependent behavior. In this regard, the system is not subjected to excitation and therefore, the motor is at rest in a specific angle θ. A locus of equilibrium points against the forcing motor phase is plotted to show the general structure of equilibrium points. The stability of each equilibrium point is analyzed assessing the eigenvalues of the Jacobian matrix. A reference situation is defined at high temperature ($T = 291.15K > T_A$)

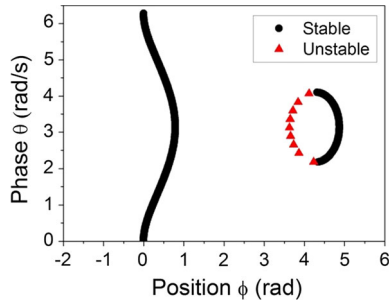

Fig. 3 Location of equilibrium points against forcing motor phase for the system with linear springs. *Triangles* are unstable fixed points and the *continuum lines* are the stable ones

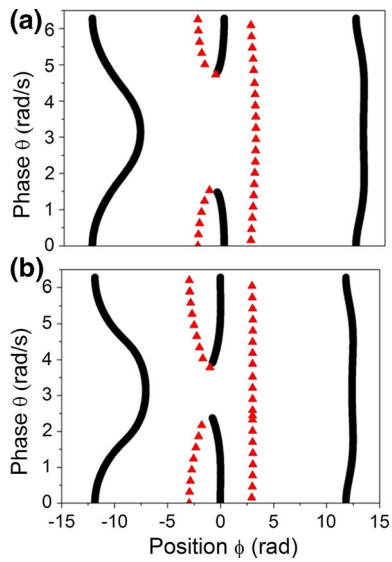

Fig. 4 Location of equilibrium points. **a** $T = 280.15\,\mathrm{K}$, below T_M. **b** $T = 283.15\,\mathrm{K}$, right above T_M. *Triangles* are unstable fixed points and the *continuum lines* are the stable ones

where results are similar to the one obtained with elastic springs and discussed in [3]. Figure 3 shows the equilibrium point locus for this case presenting regions related to just only one stable equilibrium point and a region ($2.71 \leq \theta \leq 4.11$) related to three equilibrium points (two stable and one unstable).

The influence of temperature on the structure of equilibrium point is now in focus considering the system response for different temperatures. The use of SMA springs promotes dramatic changes on system responses. Figure 4 shows low temperature situations, being related to martensitic phase. Note that there are five equilibrium points for $\theta = 0$, two of them unstable and three stable, all positioned symmetrically around the origin. By changing the motor's phase, the symmetry is broken moving the equilibrium points until stable and unstable equilibrium points collide. It should be observed that these asymmetries are introduced by the motor's phase angle θ. The increase of temperature changes the structure of equilibrium points. Figure 4b shows the movement and the growth of the ellipse arches until their separation after the end touch that occurs when.

Intermediate temperature range ($T_\mathrm{M} < T < T_\mathrm{A}$) allows both martensite and austenite to be stable and, therefore, is related to a greater number of equilibrium points. Figure 5a presents the moment after the ellipse touch described. The increase of temperature for higher levels promotes the creation of another ellipse as shown in Fig 5c, d. Further increase of the temperature causes the ellipse's growth until its separation. This is followed by the creation of another ellipse on the region of $-10\,\mathrm{rad}$ (Fig. 5e).

A new dramatic change occurs when temperature values approach to T_A (Fig. 5f). After this value, only austenite is stable in a stress-free state. At this point the ellipse structures start to contract and form by the coalescences of stable and unstable paths of equilibrium points. Here, it is important to notice that the ellipses can be formed as single, pairs or split into two while collapsing (Figs. 5f, 6a). The formation of ellipse pairs and their division is due to the constitutive nonlinearity and cannot be observed on the system with linear spring. The limit case occurs at $T = 291.15K$ where phase transformations occur for values out of the range of the pendulum dynamics and the original linear spring case presented in Fig. 3 is reached.

Experimentally speaking, it is difficult to establish a compression–tension spring. This drawback can be overcome by using an extensive spring subjected to a pre-stress. The pre-stress changes the structure of the equilibrium points, as can be seen on Fig. 7. In general, it should be highlighted that the equilibrium points structure can be designed according to the application by changing material properties represented by constitutive parameters: b_m and a_m; and phase transformation temperatures T_A and T_M. For instance, adopting $b_m = 75\,\mathrm{Pa/m}$ and $a_m = 0.4375\,\mathrm{N/mK}$, and adopting a greater value of T_A, the structure of equilibrium points become as shown in Fig. 8.

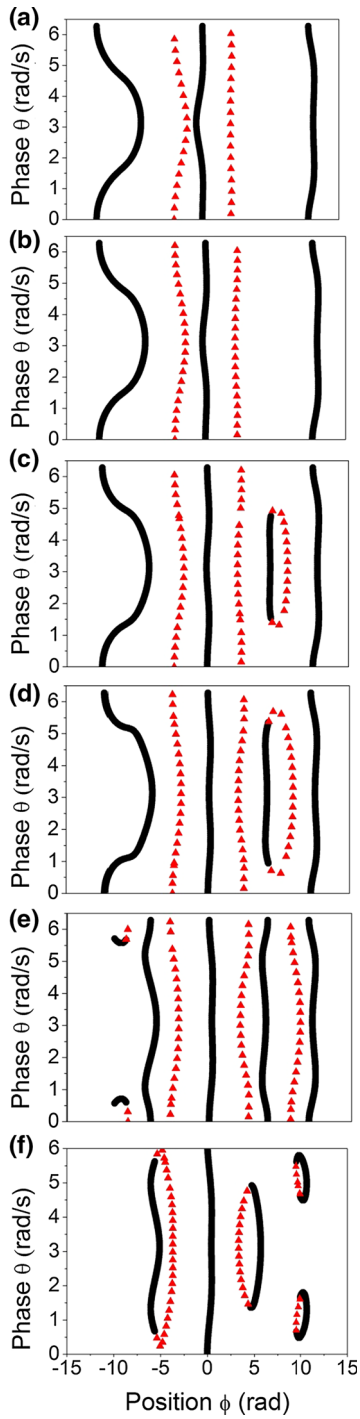

Fig. 5 Location of equilibrium points using SMA spring system for $T_M < T < T_A$. **a** $T = 284.15$ K. **b** $T = 285.15$ K. **c** $T = 286.15$ K. **d** $T = 287.15$ K. **e** $T = 288.15$ K. **f** $T = 289.15$ K. *Triangles* are unstable fixed points and the *continuum lines* are the stable ones

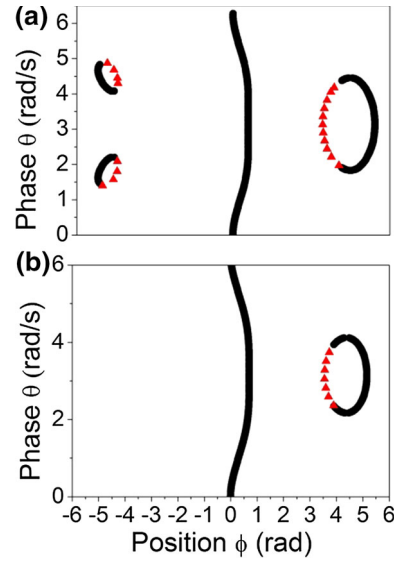

Fig. 6 Location of equilibrium points for $T > T_A$. *Triangles* are unstable fixed points and the *continuum lines* are the stable ones. **a** $T = 290.15$ K. **b** $T = 291.15$ K

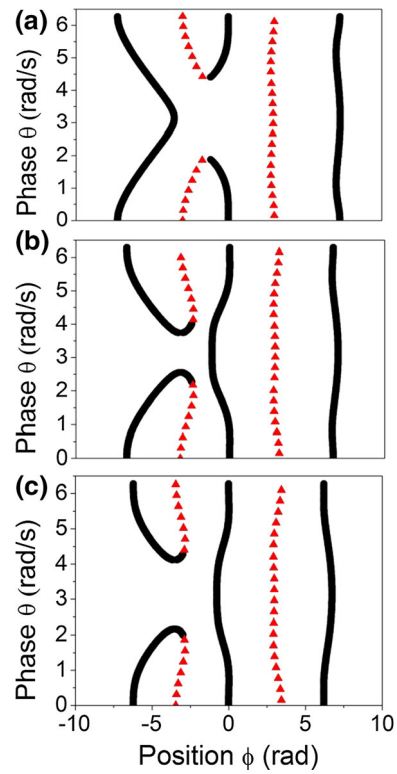

Fig. 7 Location of equilibrium points for $T_M < T < T_A$. **a** $T = 286.15$ K. **b** $T = 287.15$ K. **c** $T = 288.15$ K. *Triangles* are unstable fixed points and the *continuum lines* are the stable ones

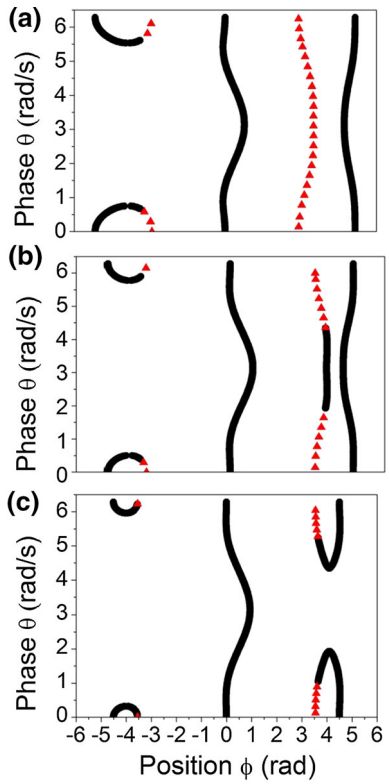

Fig. 8 Location of equilibrium points for $T > T_M$; b_m and T_A altered. **a** $T = 291.15$ K. **b** $T = 295.15$ K. **c** $T = 297.15$ K. *Triangles* are unstable fixed points and the *continuum lines* are the stable ones

4 Forced vibration

Forced vibration is now analyzed. Initially, bifurcation diagrams are of concern providing a general comprehension about the system dynamics. Figure 9 presents a bifurcation diagram showing the position under temperature variation considering forcing frequency of $\omega = 5.5$ rad/s and motor arm length $b = 0.06$ m. Diagrams are constructed eliminating the first 600 periods and assuming different initial conditions. Note that the change on temperature causes different kinds of responses. Periodic and chaotic responses are possible, and multistability can be observed since different initial conditions, $x_0 = (\phi_0, \phi_0)$, are related to different solutions. In this regard, it is important to observe the coexistence of period-1 and chaotic responses when $T = 291.15$ K (Fig. 10); period-12 and period-1 responses (Fig. 11) when $T = 283.55$. It is also noticeable that there is a periodic window around 291.15 K on Fig. 9a, b, while Fig. 9c is still related to a chaotic response.

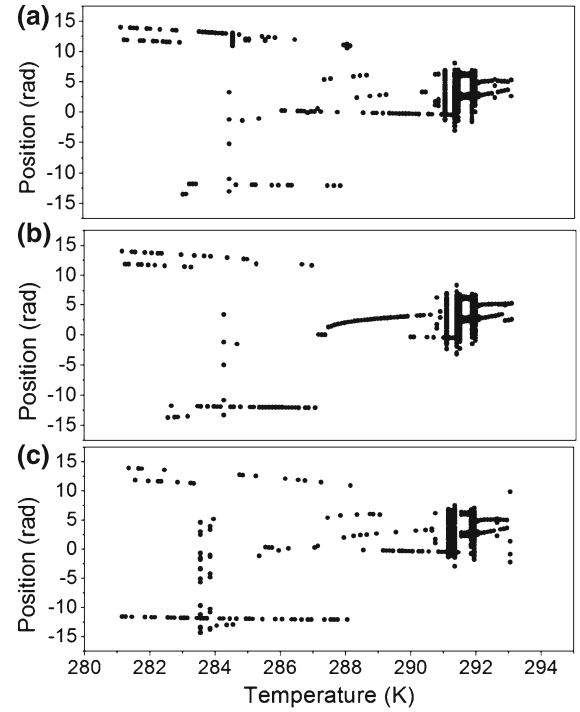

Fig. 9 Bifurcation diagram for $\omega = 5.5$ rad/s considering different initial condition. **a** $x_0 = (9, 0)$; **b** $x_0 = (0, 0)$; **c** $x_0 = (-9, 0)$

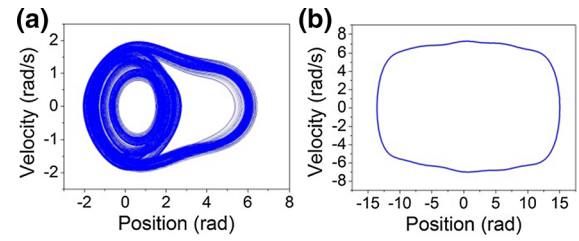

Fig. 10 Response with forcing frequency of $\omega = 5.5$ rad/s and $T = 291.15$ K. **a** Chaotic $x_0 = (3, 0)$. **b** Periodic $x_0 = (-12, 0)$

The influence of frequency variation is verified by considering a bifurcation diagram with constant temperature, $T = 291.15$ K, presented in Fig. 12. Once again, multiple chaotic regions are observed coexisting with period-1 solutions: three small chaotic-like twin regions around frequency values 4.78, 5.18 and 5.5 rad/s, and two great chaotic regions close to $\omega = 5.4$ and 6 rad/s (Fig. 12b). Differences on these chaotic regions suggest that their attractors have different structures. Note that the three first mentioned chaotic regions are always in a transition between a period-1 orbit and another orbit.

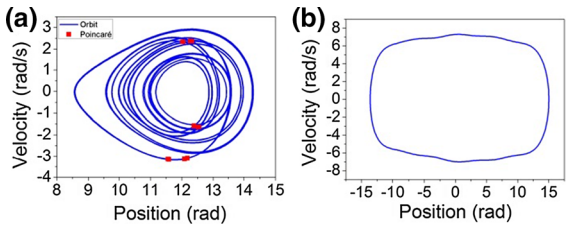

Fig. 11 Response with forcing frequency $\omega = 5.5$ rad/s and $T = 283.65$ K. **a** Period-12 $x_0 = (9, 0)$. **b** Period-1 $x_0 = (-10, 0)$

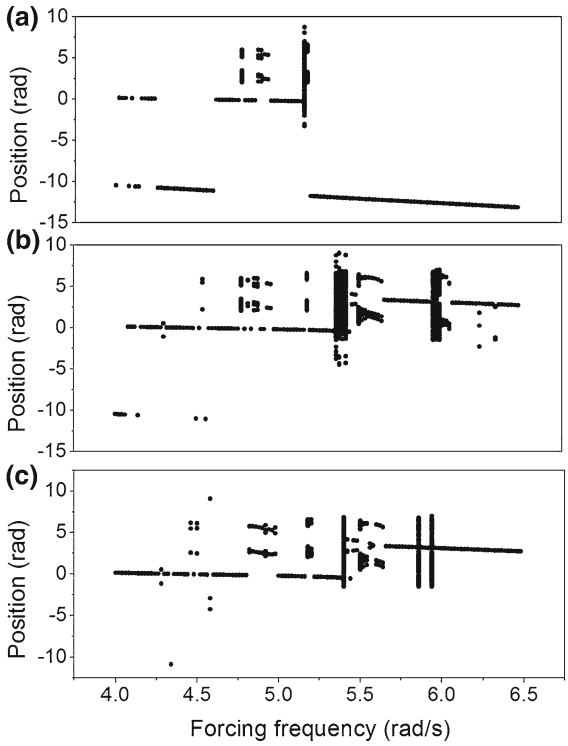

Fig. 12 Bifurcation diagram varying the forcing frequency for $T = 291.15$ K and different initial condition. **a** $x_0 = (-6, 0)$; **b** $x_0 = (-3, 0)$; **c** $x_0 = (6, 0)$

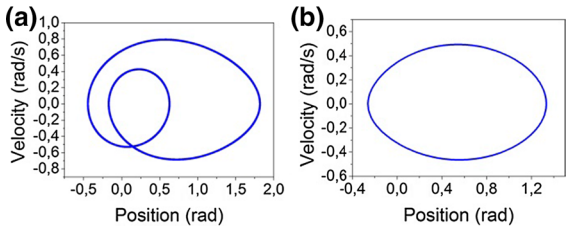

Fig. 13 System solutions on different forcing frequencies. **a** $\omega = 3.59$ rad/s, $x_0 = (0, 0)$; **b** $\omega = 5.1$ rad/s, $x_0 = (0, 0)$

Some specific behaviors are now analyzed at $T = 291.15$ K. Figure 13a presents a period-2 response for the forcing frequency $\omega = 3.59$ rad/s, while Fig. 13b

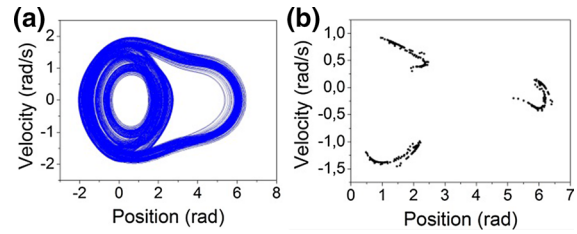

Fig. 14 Chaotic response with $\omega = 5.5$ rad/s, $x_0 = (0, 0)$. **a** Phase space. **b** Poincaré section

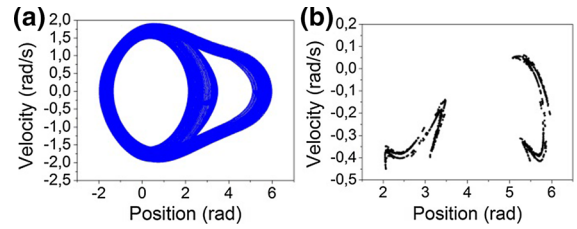

Fig. 15 Chaotic response with $\omega = 4.78$ rad/s, $x_0 = (3, 0)$. **a** Phase space. **b** Poincaré section

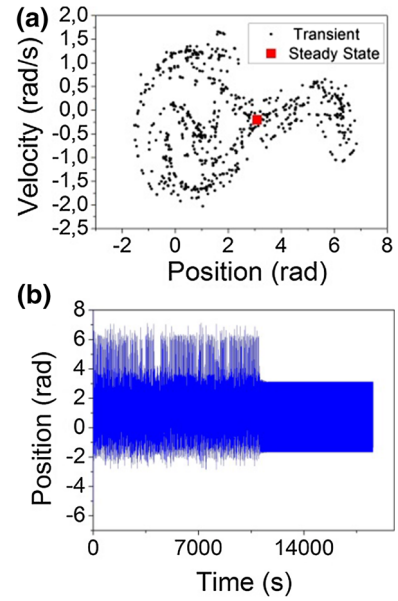

Fig. 16 Transient chaos for $\omega = 6$ rad/s, $x_0 = (10.152, 0)$. **a** Chaotic saddle and steady state. **b** Position time history

presents a period-1 response with $\omega = 5.1$ rad/s. By considering $\omega = 5.5$ rad/s, a chaotic response appears. Figure 14 shows both phase space and Poincaré map of this response that can be assured as chaotic by calculating the Lyapunov exponents using the algorithm proposed by WOLF et al. [24] that presents a positive largest value of $\lambda = 0.14 \pm 0.02$ bit/s. The Poincaré

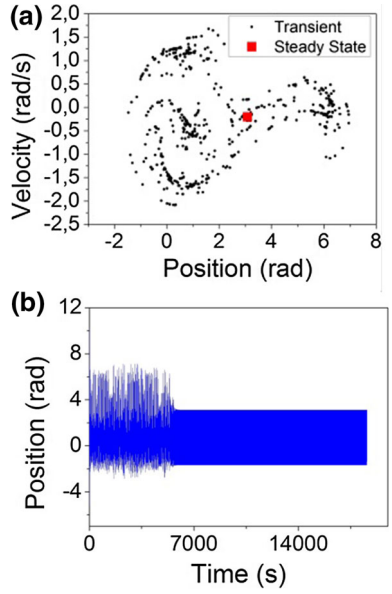

Fig. 17 Transient chaos for $\omega = 6$ rad/s, $x_0 = (10.151, 0)$. **a** Chaotic saddle and steady state. **b** Position time history

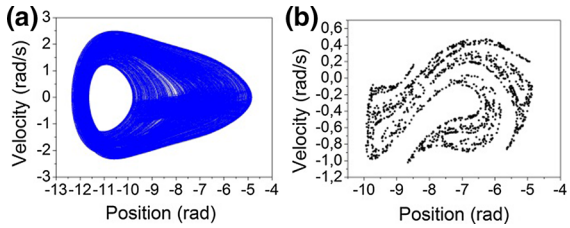

Fig. 18 Chaotic response for $T = 286.15$ K, $\omega = 6$ rad/s and $b = 0.015$ m. **a** Phase space. **b** Poincaré section

section shows a three-region disconnected fractal-like structure. Figure 15 presents a similar chaotic response considering $\omega = 4.78$ rad/s but with a two-region attractor instead of three-region of the previous case. The period-1 orbits that coexist with chaotic responses have the form of the orbits presented in Fig. 13b.

Transient chaos is an unstable chaotic response associated with a chaotic saddle. In essence, transient chaos evolution is being expelled from the chaotic saddle and therefore, the system presents a transient response. This transient behavior tends to stabilize in a periodic orbit that does not belong to the chaotic saddle. In addition, it can be related to vibrations and overshoots before the stabilization, being undesirable for some applications [25,26]. Figure 16 presents the transient chaos associated with the SMA-pendulum system, showing chaotic saddle and the time history of the response for $\omega = 6$ rad/s. Figure 17 presents the same response but with different initial conditions. Note that the steady state response is the same for both situations, but the transient is different. It is noticeable the fractal-like structure of the chaotic saddle and also that, during transient response, the system presents a positive value of the greatest Lyapunov exponent (0.52 ± 0.03 bits/s).

Due to the coexistence of chaotic and periodic orbits, it is interesting to investigate the influence of energy delivered to the system. In order to perform this analysis, motor arm length b is varied and results are plotted as a bifurcation diagram with a constant temperature $T = 286.15$ K (Fig. 19). A chaotic region around $b = 0.015$ m can be clearly identified. This solution is observed in Fig. 18 that shows the phase space and the Poincare section with largest Lyapunov exponent value $\lambda = 0.48 \pm 0.03$ bits/s. This solution coexists with two periodic orbits presented in Fig. 20. For greater values of b (out of the figure range), a chaotic region similar to an SMA oscillator studied in reference [15] is verified.

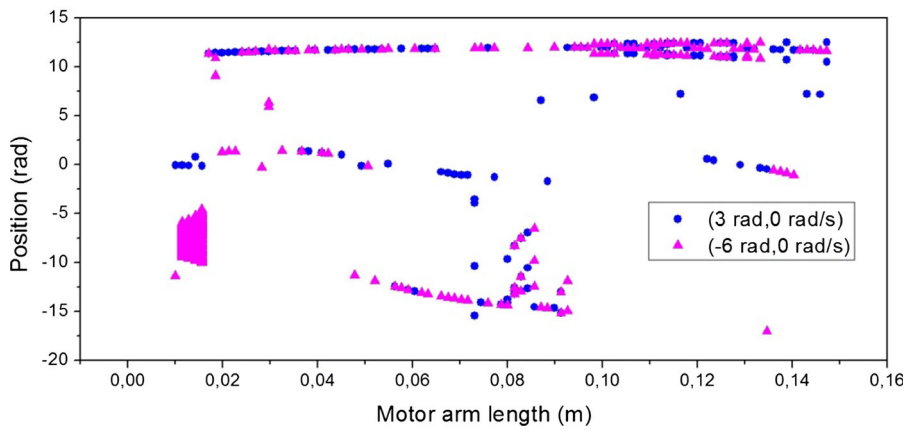

Fig. 19 Bifurcation diagram for $T = 286.15$ and forcing frequency of $\omega = 6$ rad/s against motor arm length for different initial conditions

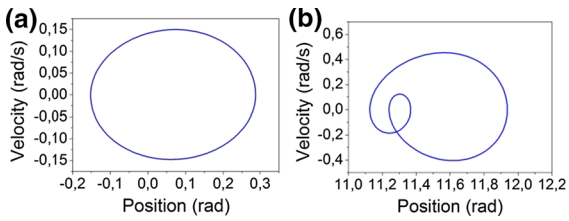

Fig. 20 Period-1 orbits coexisting with the chaotic attractor of Fig. 16. **a** Close to the origin (position $\phi = 0$). **b** Upper position ($\phi = 11.4$ rad)

The similarity is expected in situation where the SMA behavior is preponderant with respect to gravitational force.

The influence of temperature is now focused again with a motor arm b $= 0.015$ m. Figure 21 shows bifurcation diagrams for different temperature varying from $T = 284.55$ to $T = 286.15$ K (0.5 K interval), and distinct initial conditions. There are always two or more coexisting orbits, one of them being periodic. Moreover, two chaotic regions coexist on Fig. 21b. Note that, as the temperature increases, the chaotic regions are created, shifted to the left or destroyed. The chaotic region on the bottom of Fig. 21c–e also have windows of periodicity that also evolve with the chaos, "pushing" it aside, rising and growing between the chaos. Therefore, a temperature increase can be related to the appearance of chaotic regions, the creation of periodic islands between these regions, a motion induced by these periodic windows and finally the destruction of the chaos, like islands emerging in the ocean, pushing it aside and submerging again.

5 Control

The temperature-dependent behavior of SMA-pendulum system can be exploited for control purposes. One may suppress chaotic responses, stimulate changes from one periodic orbit to another or use temperature changes to suppress this dynamical response. Figure 22 illustrates a situation where temperature variation is employed to change the system global response. It is built by initializing the system at $x_0 = (-6, 0)$, forcing frequency $\omega = 6.5$ rad/s, motor arm length $b = 0.015$ m. Temperature is history assumes $T = 286.65$ K for 600 cycles. Under this condition, the system presents a chaotic response (bottom chaotic region of Fig. 21b). Afterward, the temperature

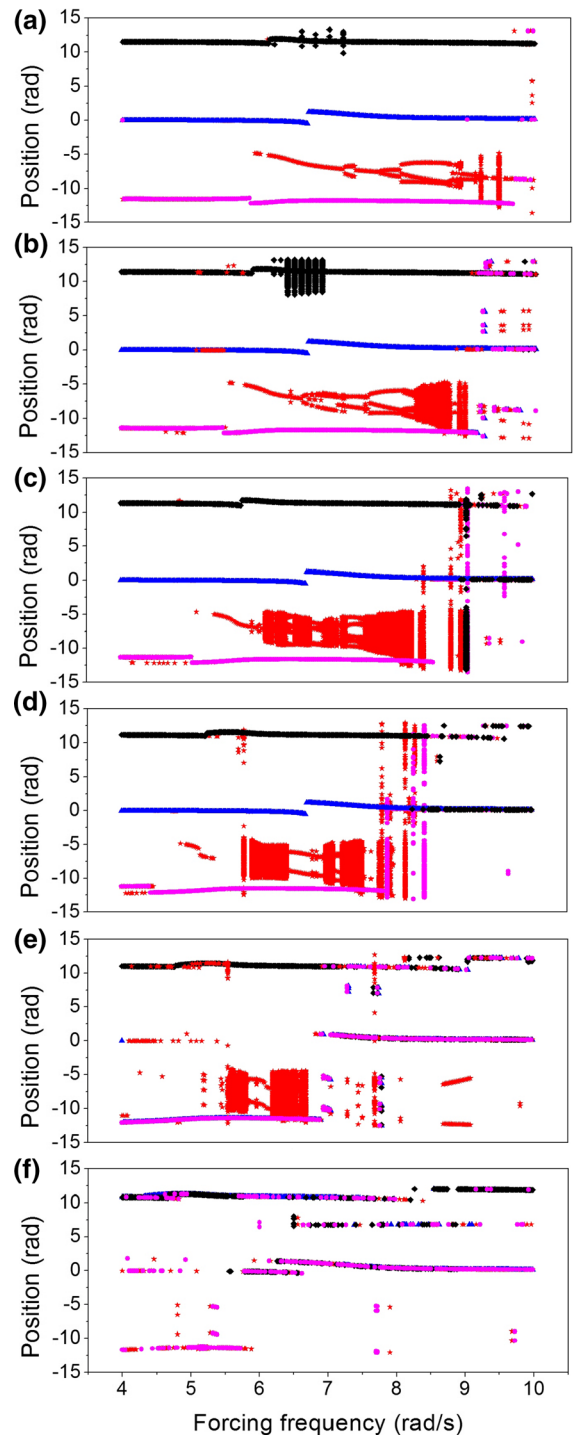

Fig. 21 Bifurcation diagrams change due to temperature variations with a motor arm length $b = 0.015$ m and different initial conditions, x_0: *circle* $(-12, 0)$; *star* $(-6, 0)$; *triangle* $(0, 0)$; *diamond* (15 rad, 0) on **a** and **b**; *diamond* $(12, 0)$ on **c**–**f**. **a** $T = 284.65$ K. **b** $T = 285.15$ K. **c** $T = 285.65$ K. **d** $T = 286.15$ K. **e** $T = 286.65$ K. **f** $T = 287.15$ K

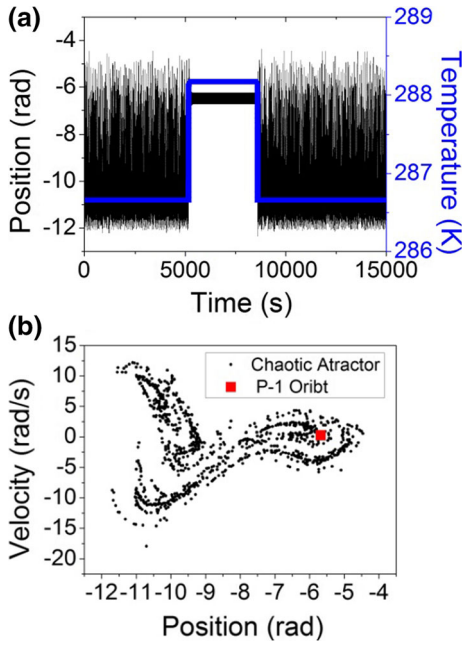

Fig. 22 Control strategy based on temperature change. **a** Chaotic-periodic-chaotic cycle. **b** Poincaré section of chaotic and periodic responses

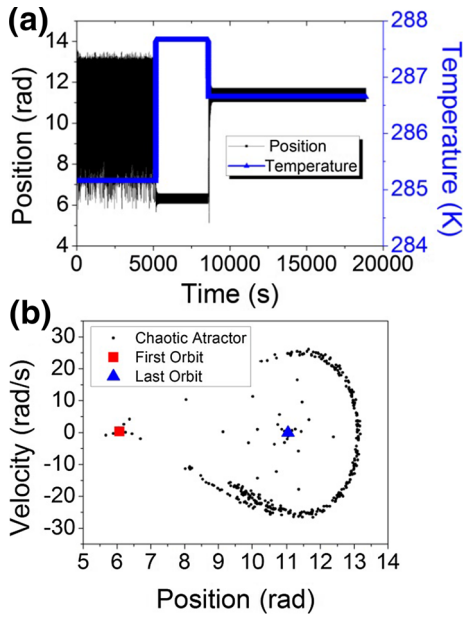

Fig. 23 Control strategy based on temperature change. **a** Chaotic-periodic-periodic cycle. **b** Poincaré section of chaotic and two periodic responses

is increased by a ramp function with linear coefficient 0.1 K/s, until it reaches $T = 288.15\,\mathrm{K}$, a temperature approaching T_A, related to a period-1 response. After 1000 cycles, the temperature is decreased to the original value, $T = 286.15\,\mathrm{K}$, and a chaotic response related to the same attractor occurs. It should be highlighted that with this control one can destroy or create the same chaotic behavior due to temperature variations.

A different control strategy is now of concern. The idea is to perform transitions between the coexisting orbits of the system. Figure 23 displays the test for this strategy. It is built by initializing the system at $x_0 = (6, 0)$, forcing frequency $\omega = 6.5\,\mathrm{rad/s}$, motor arm length $b = 0.015\,\mathrm{m}$. Temperature history starts at $T = 285.15\,\mathrm{K}$ for 600 cycles. During these cycles, the system presents a chaotic response (upper chaotic region of Fig. 21b). Afterward the temperature is increased until it reaches $T = 287.15\,\mathrm{K}$, a temperature approaching T_A, related to a period-1 response (response around 6 rad in Fig. 21f). After 1000 cycles, the temperature is decreased to $T = 286.65\,\mathrm{K}$, making the first period-1 response unstable, leading to a different period-1 orbit (response around 11 rad in Fig. 20f).

6 Conclusions

This work deals with the nonlinear dynamics of an SMA-pendulum system. The use of SMA element provides a temperature-dependent behavior introducing several possibilities related to system response. The structure of equilibrium points is discussed showing a large number of points with complex behavior altered by temperature. Concerning forced vibration, system presents several complex responses including chaos, transient chaos, multistability and high periodic orbits. All these aspects can be exploited for control purposes. Temperature variations can be employed to change either the system position or the system response in a variety of ways. These situations are exploited showing the control as a possibility to promote changes on the qualitative kind of response. The creation or suppression of chaos and the orbit changes are analyzed due to temperature variations. Basically, it is possible to use temperature variations to put the system in a desired orbit choose from coexisting solutions.

Acknowledgements The authors would like to acknowledge the support of the Brazilian Research Agencies CNPq, CAPES and FAPERJ and through the INCT-EIE (National Institute of Science and Technology - Smart Structures in Engineering)

the CNPq and FAPEMIG. The Air Force Office of Scientific Research (AFOSR) is also acknowledged.

References

1. Pilipchuk, V.N., Vakakis, A.F., Azeez, M.A.F.: Sensitive dependence on initial conditions of strongly nonlinear periodic orbits of the forced pendulum. Nonlinear Dyn. **16**(3), 223–237 (1998)
2. Franca, L.F.P., Savi, M.A.: Distinguishing periodic and chaotic time series obtained from an experimental nonlinear pendulum. Nonlinear Dyn. **26**(3), 255–273 (2001)
3. de Paula, A.S., Savi, M.A., Pereira-Pinto, F.H.I.: Chaos and transient chaos in an experimental nonlinear pendulum. J. Sound Vib. **294**(3), 585–595 (2006)
4. Bessa, W.M., de Paula, A.S., Savi, M.A.: Chaos control using an adaptive fuzzy sliding mode controller with application to a nonlinear pendulum. Chaos Solitons Fractals **42**(2), 784–791 (2009)
5. de Paula, A.S., Savi, M.A.: Controlling chaos in a nonlinear pendulum using an extended time-delayed feedback control method. Chaos Solitons Fractals **42**(5), 2981–2988 (2009)
6. Pan, Y., Zhou, Y., Sun, T., Er, M.J.: Composite adaptive fuzzy H∞ tracking control of uncertain nonlinear systems. Neurocomputing **99**, 15–24 (2013)
7. Suzuki, Y., Nomura, T., Casadio, M., Morasso, P.: Intermittent control with ankle, hip, and mixed strategies during quiet standing: a theoretical proposal based on a double inverted pendulum model. J. Theor. Biol. **310**, 55–79 (2012)
8. Chen, L., Sun, X., Jiang, H., Xu, X.: A high-performance control method of constant-controlled induction motor drives for electric vehicles. Math. Probl. Eng. **2014**, 1–10 (2014)
9. Ju, F., Choo, Y.S., Cui, F.S.: Dynamic response of tower crane induced by the pendulum motion of the payload. Int. J. Solids Struct. **43**(2), 376–389 (2006)
10. Savi, M.A.: Nonlinear dynamics and chaos in shape memory alloy systems. Int. J. Non-Linear Mech. **70**, 2–19 (2015)
11. Bessa, W.M., de Paula, A.S., Savi, M.A.: Adaptive fuzzy sliding mode control of smart structures. Eur. Phys. J. Spec. Top. **222**(7), 1541–1551 (2013)
12. Kuribayashi, K., Tsuchiya, K., You, Z., Tomus, D., Umemoto, M., Ito, T., Sasaki, M.: Self-deployable origami stent grafts as a biomedical application of Ni-rich TiNi shape memory alloy foil. Mater. Sci. Eng. A **419**(1–2), 131–137 (2006)
13. Kim, B., Lee, M.G., Lee, Y.P., Kim, Y., Lee, G.: An earthworm-like micro robot using shape memory alloy actuator. Sens. Actuators Phys. **125**(2), 429–437 (2006)
14. Lebedev, G.A., Gusarov, B.V., Viala, B., Delamare, J., Cugat, O., Lafont, T., Zakharov, D. I.: Thermal energy harvesting using shape memory/piezoelectric composites. In: Solid-State Sensors, Actuators and Microsystems Conference (TRANSDUCERS), 2011 16th International, pp. 669–670 (2011)
15. Machado, L.G., Savi, M.A., Pacheco, P.M.C.L.: Nonlinear dynamics and chaos in coupled shape memory oscillators. Int. J. Solids Struct. **40**(19), 5139–5156 (2003)
16. Machado, L.G., Savi, M.A.: Medical applications of shape memory alloys. Braz. J. Med. Biol. Res. **36**(6), 683–691 (2003)
17. Piccirillo, V., Balthazar, J.M., Jr. Pontes, B.R , Felix, J.L.P.: Chaos control of a nonlinear oscillator with shape memory alloy using an optimal linear control: part I: ideal energy source. Nonlinear Dyn. **55**(1–2), 139–149 (2009)
18. Arrieta, A.F., Hagedorn, P., Ertuk, A., Inman, D.J.: A piezoelectric bistable plate for nonlinear broadband energy harvesting. Appl. Phys. Lett. (2010). doi:10.1063/1.3487780
19. Silva, L.L., Oliveira, S.A., Pacheco, P.M.L.C., Savi, M.A.: Synergistic use of smart materials for vibration-based energy harvesting. Eur. Phys. J. Spec. Top. **224**(14–15), 3005–3012 (2015)
20. Aguiar, R.A.A., Savi, M.A., Pacheco, P.M.C.L.: Experimental and numerical investigations of shape memory alloy helical springs. Smart Mater. Struct. **19**(2), 25008 (2010)
21. Lagoudas, D.C.: Shape Memory Alloys, vol. 1, 1st edn. Springer US, Boston (2008)
22. Paiva, A., Savi, M.A., Braga, A.M.B., Pacheco, P.M.C.L.: A constitutive model for shape memory alloys considering tensile-compressive asymmetry and plasticity. Int. J. Solids Struct. **42**(11–12), 3439–3457 (2005)
23. Enemark, S., Santos, I.F., Savi, M.A.: Modelling, characterisation and uncertainties of stabilised pseudoelastic shape memory alloy helical springs. J. Intell. Mater. Syst. Struct. (2016). doi:10.1177/1045389X16635845
24. Wolf, A., Swift, J.B., Swinney, H.L., Vastano, J.A.: Determining Lyapunov exponents from a time series. Phys. D **16**, 285–317 (1985)
25. Sinou, J.-J.: Transient non-linear dynamic analysis of automotive disc brake squeal—on the need to consider both stability and non-linear analysis. Mech. Res. Commun. **37**(1), 96–105 (2010)
26. Monroe, R.J., Shaw, S.W.: Nonlinear transient dynamics of pendulum torsional vibration absorbers—part I: theory. J. Vib. Acoust. (2013). doi:10.1115/1.4007561